

Equivalent Series Resistance-Based Energy Loss Analysis of A Battery Semi-Active Hybrid Energy Storage System

Chen Zhao, *Student Member, IEEE*, He Yin, *Student Member, IEEE*,
Zhongping Yang, *Member, IEEE*, Chengbin Ma, *Member, IEEE*,

Abstract—This paper provides a theoretical analysis on the energy loss of a battery-ultracapacitor hybrid energy storage system based on the equivalent series resistances and a pulsed current load profile. The optimal current distribution that minimizes the overall energy loss is proved to be solely determined by the ratio of internal resistances between battery and ultracapacitor packs. Due to a large difference in the internal resistances, a quasi-optimal current distribution can be considered to let the battery pack provide the average load current, and ultracapacitor pack supply the entire dynamic load current. This result clearly demonstrates that the ultracapacitor pack should supply most of the dynamic load current not only because of battery protection, but also for energy loss minimization. Finally, the theoretical analysis is validated by both simulation and experimental results. Additional discussions such as sensitivity analysis, the influence of the sizing of ultracapacitors and a realistic test cycle are also added for reference purposes.

Index Terms—Ultracapacitor, lithium-ion battery, hybrid energy storage system, energy loss, equivalent series resistance

I. INTRODUCTION

BATTERY-ULTRACAPACITOR hybrid energy storage systems (HESSs) have been widely investigated in recent years. The basic concept is to use ultracapacitors (UCs) as an assistive energy storage device to improve the efficiency, reliability, and dynamic response of the battery-based energy storage systems. This also avoids the necessity of an oversized battery pack [1]–[4]. The absence of chemical reactions results in long cycle-life of UCs. Besides, for constant power discharges with a 10% reduction in energy capacity, the power density of most UCs is greater than 1000 W/kg, while the power density for 95% efficiency of discharge varies from about 700 to over 2500 W/kg [5]. Both of the power densities are higher by a factor of 2-3 than those of most batteries. The operating temperature range of UCs (-40 to +70°C) is also wider than that of batteries. In addition, the state of charge

(SOC) of an UC can be easily detected due to the obvious fact that its SOC is proportional with the square of the cell voltage. However, the primary disadvantage of UCs is their low energy density compared to batteries. The energy density of the symmetric UCs is 3-5 Wh/kg and that of the non-symmetric ones is 10-12 Wh/kg, compared to 100-170 Wh/kg for the batteries [5]. Hybridization of batteries and UCs is considered to be the best usage of UCs in real applications that provides high energy density, long cycle life, and low cost [5], [6].

There are mainly three different types of the battery-ultracapacitor HESSs: passive, semi-active, and fully active hybrids [7]. The passive hybrid is the most common and simplest hybrid topology, in which battery and UC packs are directly connected in parallel [8], [9]. For active hybrids, DC-DC converters are employed to control the distribution of load current between the battery and UC packs [10], [11]. Various configurations are possible with different number and placement of the DC-DC converters [7]. Many energy management strategies have been proposed in order to improve the energy efficiency of the HESS and the life expectancy of batteries. An optimal-control-model approach was discussed and implemented in real time using Neural Networks [12]. A wavelet-transform algorithm was introduced to identify the high frequency power transients and allocate power flow [13]. Rule-based approach and fuzzy logic were shown to be suitable for the control of the HESS [14]–[16]. Model predictive control is able to handle various constraints in the HESS [16], while future load demands can be predicted by using a probability-weighted Markov process in order to facilitate an optimal control [17]. The trade-off relationship between battery protection and energy loss minimization can be addressed using a multi-objective optimization approach [18].

Meanwhile, as to the knowledge of the authors, there is a lack of a general discussion on the energy loss of the battery-ultracapacitor HESS that does not depend on any specific control algorithm or physical limitations. This discussion is important to establish a guideline for evaluation and improvement on the management of the HESS. It is found and proved that the optimal distribution of load current between battery and UC packs is solely determined by the ESR (equivalent series resistance) ratio between battery pack and UC pack, which minimizes the overall energy loss of the HESS. Finally, the theoretical analysis is validated by both simulation and experiments. Further discussions are also provided on the

Manuscript received September 30, 2014; revised January 23, 2015; accepted March 20, 2015. This work was supported by National Science Foundation of China under Grant 50950110341 (2010) and Grant 51375299 (2014-2017), and Nippon Chemi-con Corporation.

C. Zhao and H. Yin are with the University of Michigan-Shanghai Jiao Tong University Joint Institute, Shanghai Jiao Tong University, Shanghai 200240, China (e-mail: zc437041363@sjtu.edu.cn; yyy@sjtu.edu.cn).

Z. Yang is with School of Electrical Engineering, Beijing Jiao Tong University, Beijing, P. R. China (email: zhpyang@bjtu.edu.cn).

C. Ma is with the University of Michigan-Shanghai Jiao Tong University Joint Institute, Shanghai Jiao Tong University, Shanghai 200240, China; and also with the School of Mechanical Engineering, Shanghai Jiao Tong University, Shanghai, China (e-mail: chbma@sjtu.edu.cn).

influences of sizing and a realistic test cycle.

II. SYSTEM MODELING

A. System Configuration

Various topologies of the battery-UC HESS are compared in [7]. With a single DC-DC converter, two semi-active topologies are possible, i.e., capacitor semi-active and battery semi-active hybrids. In the capacitor semi-active hybrid topology a DC-DC converter is connected between the UC pack and the load, while in the battery semi-active hybrid topology the DC-DC converter is placed between the battery and the load. The battery semi-active hybrid is capable of controlling the battery working at near-average load power, therefore reducing the power rating of the DC-DC converter [2], [7], [19]. This topology also allows potential improvement in battery performance such as increased lifetime and energy efficiency [7], [20]. Here the battery semi-active topology is used as an example to facilitate the theoretical analysis. Meanwhile, the methodology developed below itself is general that can be extended to analyze other battery-ultracapacitor HESS topologies such as the ultracapacitor semi-active topology.

B. Dynamic Models

The energy loss of the battery semi-active HESS includes the losses from the battery pack, the DC-DC converter, and the UC pack. Their dynamic models are first discussed for the following theoretical analysis and simulation.

1) *Lithium-ion battery pack*: In this system-level analysis, the equivalent circuit model is used for the lithium-ion battery pack, as shown in Fig. 1. $V_{o,b}$ is the open circuit voltage (OCV) of the battery and R_s is the battery internal resistance. The two RC networks with different time constants, $\tau_s = R_{t,s}C_{t,s}$ and $\tau_m = R_{t,m}C_{t,m}$, model the transient voltage responses of the battery in second and minute ranges, respectively [21]. $V_{o,b}$ and R_s are represented by the sixth-order polynomials

$$V_{o,b} = a_0 + a_1x + a_2x^2 + \dots + a_6x^6, \quad (1)$$

$$R_s = b_0 + b_1x + b_2x^2 + \dots + b_6x^6, \quad (2)$$

where x is a specific SOC [22]. The parameters of the two RC networks, $R_{t,s}$, $C_{t,s}$, $R_{t,m}$, $C_{t,m}$ are assumed to be constant. Because R_s is usually much larger than $R_{t,s}$ and $R_{t,m}$, the power loss of the battery pack $P_{loss,b}$ can be approximately written as

$$P_{loss,b} = R_s i_{b,rms}^2 + \frac{V_{t,m,rms}^2}{R_{t,m}} + \frac{V_{t,s,rms}^2}{R_{t,s}} \approx R_s i_{b,rms}^2, \quad (3)$$

where $i_{b,rms}$ is the battery Root Mean Square (RMS) current. It is known that the performance of the lithium-ion batteries is affected by temperature and aging, which in turn leads to the variation in battery internal resistance R_s [23]. As discussed in the following sections, R_s is a key factor to affect the optimal current distribution in the HESS.

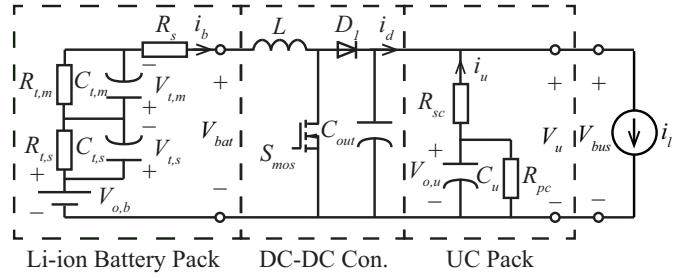


Fig. 1. Dynamic model for the battery semi-active HESS used in simulation.

2) *Ultracapacitor pack*: Again for system-level analysis, the first-order electrical model is sufficient to represent the behavior of the UC pack [24] [see Fig. 1]. $V_{o,u}$ is the OCV of the UC pack. R_{sc} is its internal resistance and R_{pc} models the leak current [25]. The UC capacitance C_u depends on UC voltage V_u . Because R_{pc} is usually large, the power loss of the UC pack $P_{loss,u}$ can be approximately represented as

$$P_{loss,u} = R_{sc} i_{u,rms}^2 + \frac{V_{o,u,rms}^2}{R_{pc}} \approx R_{sc} i_{u,rms}^2, \quad (4)$$

where $i_{u,rms}$ is the UC RMS current.

3) *DC-DC converter*: A current-mode controlled boost converter is used in the experimental battery semi-active HESS [see Fig. 1]. Its power loss $P_{loss,d}$ can be approximately calculated using the first-order model of DC-DC converter [26], [27]. In the model, switching duty cycle d_s and inductor RMS current $i_{L,rms}$ are used to estimate the losses in MOSFET switch S_{mos} , diode D_1 , and inductor L . Because the gate drive power loss of the DC-DC converter is usually small, the power loss can be expressed as

$$\begin{aligned} P_{loss,d} &= V_{in} f_s Q_{mos} + (d_s R_{mos} + R_L) i_{L,rms}^2 \\ &\quad + R_{D1} i_{d,rms}^2 + V_F i_{d,ave} \\ &\approx (d_s R_{mos} + R_L) i_{L,rms}^2 + R_{D1} i_{d,rms}^2 + V_F i_{d,ave}, \end{aligned} \quad (5)$$

where V_{in} is the input voltage of the DC-DC converter; f_s is the switching frequency of the DC-DC converter; Q_{mos} is the gate charge of the MOSFET switch S_{mos} ; $i_{d,rms}$ and $i_{d,ave}$ are the RMS and average values of the output current of the DC-DC converter, respectively; R_{mos} is the on-resistance of S_{mos} ; R_L is the ESR of the inductor L . The energy loss of the diode D_1 is caused by its voltage drop V_F and resistance R_{D1} . The parameter values of the DC-DC converter are also listed in Table II.

III. CURRENT DISTRIBUTION UNDER PULSED LOAD

Here for a theoretical analysis, a pulsed current load profile is used to represent a dynamic power profile [7], [19]. As shown in Fig. 2, the pulsed load current i_l can be decomposed into two components, average current $I_{l,a}$ and dynamic current $i_{l,d}$. $I_{l,max}$ and $I_{l,min}$ are the maximum and minimum load currents, respectively. T is the period and D is the duty cycle of the pulsed current load. The average load current $I_{l,a}$ is

$$I_{l,a} = \frac{1}{T} \int_0^T i_l dt = (1 - D) I_{l,min} + D I_{l,max}; \quad (6)$$

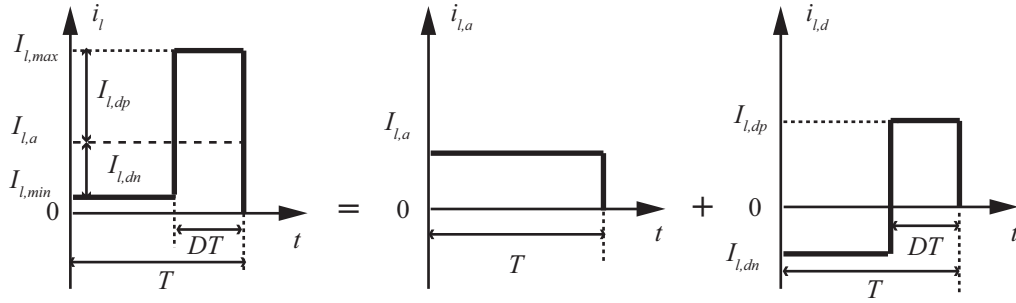


Fig. 2. The decomposition of the pulsed current load during a single period.

therefore, the dynamic current $I_{l,dp}$ and $I_{l,dn}$ are

$$\begin{aligned} I_{l,dp} &= I_{l,max} - I_{l,a} > 0, \\ I_{l,dn} &= I_{l,min} - I_{l,a} < 0, \end{aligned}$$

respectively. In order to minimize the overall energy loss of the HESS, the load current needs to be properly distributed between the battery and the UC packs. Because the UC pack is a temporary energy source, the average current $I_{l,a}$ (i.e., the average power) should be supplied by the battery pack and the dynamic current can be jointly supplied by the battery and UC packs. Here a new coefficient C_d is defined to describe the current distribution, i.e., the ratio of the dynamic current provided by the battery pack (through the DC-DC converter) to the total dynamic current in the pulsed current load,

$$C_d \triangleq \frac{I_{d,max} - I_{l,a}}{I_{l,dp}} = \frac{I_{d,min} - I_{l,a}}{I_{l,dn}}, \quad (7)$$

where $I_{d,max}$ and $I_{d,min}$ are the maximum and minimum currents of the DC-DC converter, respectively. As shown in Fig. 3, the currents of the DC-DC converter i_d and UC pack i_u during a single period can be further written as

$$i_d = \begin{cases} I_{d1} = I_{l,a} + C_d I_{l,dn} & \text{if } 0 < t \leq (1-D)T, \\ I_{d2} = I_{l,a} + C_d I_{l,dp} & \text{else,} \end{cases} \quad (8)$$

$$i_u = \begin{cases} I_{u1} = (1-C_d)I_{l,dn} & \text{if } 0 < t \leq (1-D)T, \\ I_{u2} = (1-C_d)I_{l,dp} & \text{else.} \end{cases} \quad (9)$$

A small C_d means that the UC pack provides most of the dynamic load current and thus the battery pack mainly supplies the average load current through the DC-DC converter or vice versa. An optimal C_d^* is accurately derived as follows that minimizes the overall energy loss in the battery semi-active HESS.

A. Equivalent Series Resistances

As shown in Fig. 4, the overall power loss P_{loss} of the HESS can be represented as

$$P_{loss} = i_d^2(R_b^* + R_d^*) + i_u^2 R_u^*, \quad (10)$$

where “*” denotes an ESR in terms of energy loss.

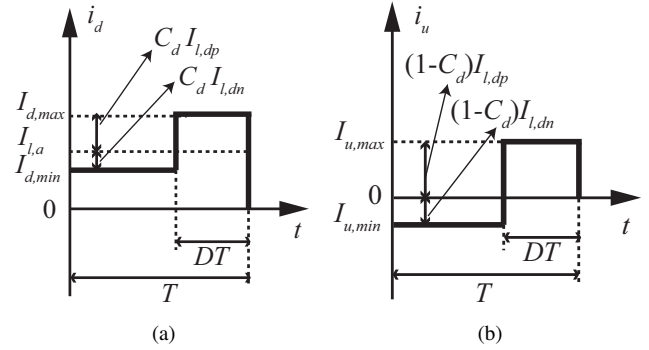


Fig. 3. The current distribution during a single period. (a) Current from DC-DC converter. (b) Current from UC pack.

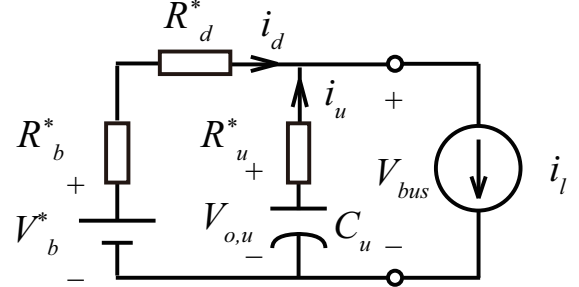


Fig. 4. ESR circuit for the battery semi-active HESS.

From (5) in which $i_d = (1-d_s)i_L$ and $i_b = i_L$, the ESR of the DC-DC converter R_d^* can be calculated as

$$\begin{aligned} R_d^* &= \frac{P_{loss,d}}{i_d^2} \approx \frac{R_L + d_s R_{MOS}}{(1-d_s)^2} + R_{D1} + \frac{V_F}{i_d} \\ &= R_{d,r}^* + \frac{V_F}{i_d}. \end{aligned} \quad (11)$$

Similarly, the ESRs of battery and UC packs, R_b^* and R_u^* , are

$$R_b^* = \frac{P_{loss,b}}{i_d^2} \approx \frac{i_b^2 R_s}{i_d^2} = \frac{R_s}{(1-d_s)^2}, \quad (12)$$

$$R_u^* = \frac{P_{loss,u}}{i_u^2} \approx R_{sc}, \quad (13)$$

respectively. The assumptions are summarized below that simplify the theoretical analysis:

- (1) The energy loss of battery pack is mainly caused by its series resistance R_s ;

- (2) The energy loss of UC pack is mainly caused by its series resistance R_{sc} ;
- (3) The duty cycle of DC-DC converter is nearly constant;
- (4) DC bus voltage is nearly constant and equal to the initial voltage of the UC pack.

B. Optimal Current Distribution

From (10)-(13), the overall power loss can be written as

$$P_{loss} = i_d^2 R_b^* + i_d^2 R_{d,r}^* + i_d V_F + i_u^2 R_u^*. \quad (14)$$

Using (8) and (9), the energy loss of the battery semi-active HESS is obtained by integrating P_{loss} during period T :

$$E_{loss} = (I_{l,a}^2 - C_d^2 I_{l,dp} I_{l,dn})(R_b^* + R_{d,r}^*)T + I_{l,a} V_F T - (1 - C_d)^2 I_{l,dp} I_{l,dn} R_u^* T. \quad (15)$$

E_{loss} can be further rewritten as

$$E_{loss} = -I_{l,dp} I_{l,dn} (R_b^* + R_{d,r}^* + R_u^*) \left(C_d - \frac{1}{1+K} \right)^2 T - I_{l,dp} I_{l,dn} R_p^* T + I_{l,a}^2 (R_b^* + R_{d,r}^*) T + I_{l,a} V_F T, \quad (16)$$

where K and R_p^* are defined as

$$K = \frac{R_b^* + R_{d,r}^*}{R_u^*}, \quad (17)$$

$$R_p^* = \frac{(R_{d,r}^* + R_b^*) R_u^*}{R_{d,r}^* + R_b^* + R_u^*}, \quad (18)$$

respectively. Note that $I_{l,dn}$ is a negative current, i.e., the regenerative current. It is interesting to notice that in (16) the optimal current distribution coefficient C_d^* is irrelevant to the level and duty cycle of the pulsed current load, but solely determined by a single parameter K , the ESR ratio of the DC-DC converter and the battery pack to the UC pack.

In real applications, there are limits on the DC bus voltage variation, and lithium-ion batteries have a flat voltage profile [7]. Therefore it is reasonable to assume a nearly constant duty cycle d_s for the DC-DC converter. Based on the dynamic model in Fig. 1, d_s can be calculated as

$$d_s = 1 - \frac{V_{o,b} + \sqrt{V_{o,b}^2 - 4R_s I_{l,a} V_{bus}}}{2V_{bus}}. \quad (19)$$

Then the ESR ratio K is

$$K = \frac{R_s}{(1-d_s)^2} + \frac{R_L + d_s R_{MOS}}{(1-d_s)^2} + R_{D1}, \quad (20)$$

and the optimal coefficient C_d^* is

$$C_d^* = \frac{1}{1+K}. \quad (21)$$

In practical battery-ultracapacitor HESSs, the ESRs of the DC-DC converter and the battery pack are usually much bigger than that of the UC pack. This corresponds to a close-to-zero optimal C_d^* . Then a quasi-optimal current distribution can be considered to simply let $C_d^* = 0$, i.e., the battery pack only provides the average load current $I_{l,a}$ through DC-DC converter. This result is significant because it is theoretically proved that besides battery protection, even for minimizing the energy loss the UC pack should also provide most of dynamic load current.

C. RMS-value-based Analysis

The above theoretical analysis and conclusions are based on the assumption of a constant duty cycle of the DC-DC converter. In practice the duty cycle varies with the changing output current of the DC-DC converter. In order to drop this assumption, RMS currents are used below to further generalize the theoretical analysis [28]. Under the pulsed current load, the battery RMS current $I_{b,rms}$ is

$$I_{b,rms} = \sqrt{\frac{(1-D)I_{d1}^2}{(1-d_{s1})^2} + \frac{DI_{d2}^2}{(1-d_{s2})^2}}, \quad (22)$$

where I_{d1} and d_{s1} are the output current and the duty cycle of the DC-DC converter when $0 < t < (1-D)T$; I_{d2} and d_{s2} are for $(1-D)T < t < T$. I_{d1} and I_{d2} are defined in (8). Again the duty cycles, d_{s1} and d_{s2} , can be derived as

$$d_{s1} = 1 - \frac{V_{o,b} + \sqrt{V_{o,b}^2 - 4R_s I_{d1} (V_{bus} - I_{u1} R_{sc})}}{2(V_{bus} - I_{u1} R_{sc})}, \quad (23)$$

$$d_{s2} = 1 - \frac{V_{o,b} + \sqrt{V_{o,b}^2 - 4R_s I_{d2} (V_{bus} - I_{u2} R_{sc})}}{2(V_{bus} - I_{u2} R_{sc})}, \quad (24)$$

where I_{u1} and I_{u2} are defined in (9). Then (22) can be further represented as (25).

Similarly, the output RMS current of the DC-DC converter $I_{d,rms}$ and UC RMS current $I_{u,rms}$ are

$$I_{d,rms} = \sqrt{I_{l,a}^2 - C_d^2 I_{l,dp} I_{l,dn}}, \quad (26)$$

$$I_{u,rms} = \sqrt{-(1-C_d)^2 I_{l,dp} I_{l,dn}}. \quad (27)$$

Then the overall energy loss in (16) can be rewritten as follows,

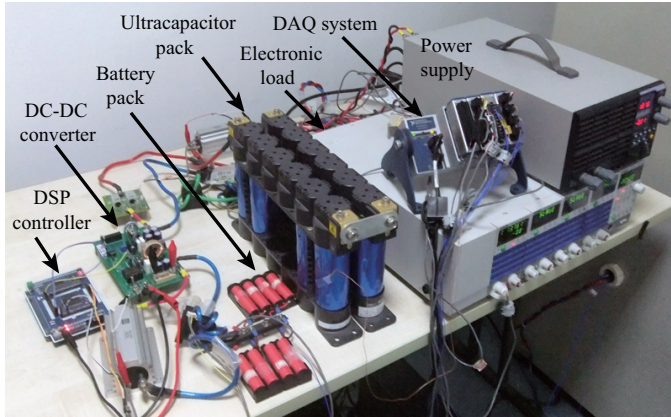
$$\begin{aligned} E_{loss} &= I_{d,rms}^2 (R_b^t + R_{d,r}^t) T + I_{u,rms}^2 R_{sc} T + I_{l,a} V_F T, \\ &= -I_{l,dp} I_{l,dn} (R_b^t + R_{d,r}^t + R_{sc}) \left(C_d - \frac{1}{1+K^t} \right)^2 T \\ &\quad - I_{l,dp} I_{l,dn} R_p^t T + I_{l,a}^2 (R_b^t + R_{d,r}^t) T + I_{l,a} V_F T, \end{aligned} \quad (28)$$

$$I_{b,rms} = \sqrt{\frac{V_{o,b}^2}{2R_s^2} - \frac{I_{l,a} V_{bus}}{R_s} - \frac{C_d(1-C_d)I_{l,dp}I_{l,dn}R_{sc}}{R_s} - \frac{(1-D)V_{o,b}}{2R_s^2} \sqrt{V_{o,b}^2 - 4R_s I_{d1} V_{bus1}} - \frac{DV_{o,b}}{2R_s^2} \sqrt{V_{o,b}^2 - 4R_s I_{d2} V_{bus2}}} \quad (25)$$

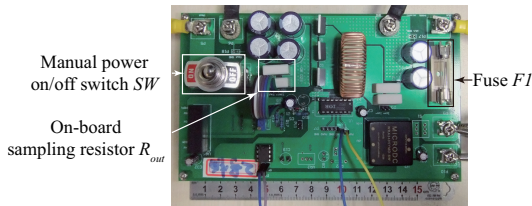
where,

$$\begin{aligned} R_b^t &= \frac{I_{b,rms}^2}{I_{d,rms}^2} R_s, R_{d,r}^t = \frac{I_{b,rms}^2}{I_{d,rms}^2} (R_L + d_s^t R_{mos}) + R_{D1}, \\ d_s^t &= \frac{1}{I_{b,rms}^2} \left[\frac{d_{s1} I_{d1}^2 (1-D)}{(1-d_{s1})^2} + \frac{d_{s2} I_{d2}^2 D}{(1-d_{s2})^2} \right], \\ K^t &= \frac{R_b^t + R_{d,r}^t}{R_{sc}}, R_p^t = \frac{(R_{d,r}^t + R_b^t) R_{sc}}{R_{d,r}^t + R_b^t + R_{sc}}. \end{aligned} \quad (29)$$

Thus K in (21) needs to be updated as K^t for calculating the optimal C_d^* here. It can be seen that with the changing duty cycle the modified ESRs of the battery pack and DC-DC converter, R_b^t and $R_{d,r}^t$, both relate to C_d . Thus the resistance ratio K^t is not constant anymore and its value is also coupled to C_d [refer to (25)-(27)]. As shown in the above equations from (22)-(29), it is difficult to get the analytical solution of the optimal C_d^* when dropping the assumption of the constant duty cycle of the DC-DC converter. For a general load profile the derivation of C_d^* becomes more challenging due to the changing RMS values of the currents. At the same time, in real applications because RMS currents can be directly measured, a new optimal control method could be developed by calculating and implementing the optimal C_d^* in real time.



(a)



(b)

Fig. 5. Experimental battery-ultracapacitor HESS. (a) System configuration. (b) DC-DC converter.

IV. SIMULATION AND EXPERIMENTAL RESULTS

A. Experimental Setup

Fig. 5 shows the experimental setup for the example battery semi-active HESS. The specifications of its major components are listed in Table I. As shown in the blockdiagram, Fig. 6, the power supply and the electronic load are controlled by a PC to emulate charging current I_{ch} and discharging current

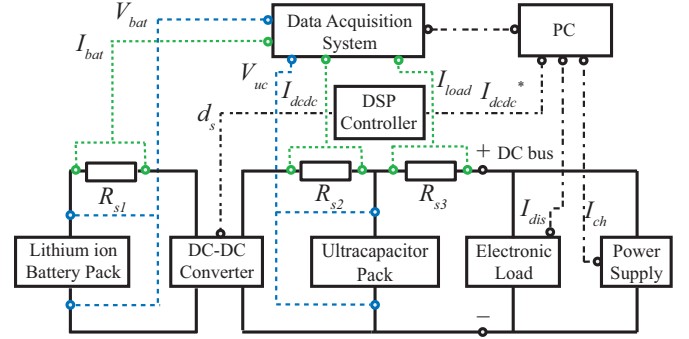


Fig. 6. The topology and control blockdiagram of the experimental battery semi-active HESS.

I_{dis} , respectively. The PC also provides reference signal I_{dc}^* to a DSP (digital signal processor) controller that controls the output current of the DC-DC converter, I_{dc} . The data acquisition (DAQ) system collects the data including battery voltage V_{bat} , UC voltage V_{uc} , battery current I_{bat} , I_{dc} , and load current I_{load} . Two 0.01Ω high-accuracy sampling resistors, R_{s1} and R_{s3} , are used to measure I_{bat} and I_{load} . I_{dc} is measured using a 0.1Ω sampling resistor R_{s2} (two 0.2Ω high-accuracy resistors connected in parallel). In order to verify the previous ESR-based theoretical discussion, the experimental HESS is configured to meet the four basic assumptions as much as possible [refer to section III-A].

TABLE I
SPECIFICATIONS FOR MAJOR COMPONENTS

Battery Pack (Sanyo 18650 Li-ion battery)	Eight cells (2 Series 4 Parallel) 2.5Ah/cell, 3.7V/cell (Nominal Voltage)
UC Pack (Nippon Chemi-Con DLE series)	Eight cells (8 Series 1 Parallel) 2300F/cell, 2.5V/cell (Max Voltage)
Power Supply (Takasago ZX-800L)	Max Power: 800W (0–80V, 0–80A)
Electronic Load (Kikusui PLZ-50F/150U)	Max Power: 600W (1 PLZ-50F, 4 PLZ150Us with 1.5–150V, 0–30A each)
DC-DC Converter (Design/fabricate in house)	Max Power: 80W Efficiency: > 90%, Size: 100mm×170mm
DAQ System (NI compactDAQ)	Two A/D boards: NI 9219
High-accuracy Sampling Resistor (PCN Corporation RH series)	Two RH250M4 0.01Ω ($\pm 0.02\%$) Two RH25E4 0.2Ω ($\pm 0.1\%$)

A detailed PSIM-based simulation model is built for the experimental HESS. The dynamic models of the battery pack, the DC-DC converter, and the UC pack in Section II-B are used in the simulation. All the model parameters are summarized in Table II. For the battery and UC packs their parameters are obtained using fast averaging method and pulsed current test, respectively [29], [30]. The additional resistors in the real experimental system affect the calculation accuracy of the duty cycle of the DC-DC converter d_s and the ESR ratio K . Besides the three high-accuracy sampling resistors, R_{s1} , R_{s2} , and R_{s3} , used by the DAQ system, the DSP controller samples the output current of the DC-DC converter through an

TABLE II
PARAMETERS FOR THE BATTERY-ULTRACAPACITOR HESS.

Battery Pack (2S4P)											
a_0	7.215	a_1	-0.161	a_2	12.326	a_3	-48.125	a_4	82.566	a_5	-64.764
a_6	19.298	b_0	0.158	b_1	-0.147	b_2	-1.337	b_3	9.612	b_4	-22.462
b_5	22.377	b_6	-8.077	$R_{t,s}$	15 m Ω	$C_{t,s}$	10000 F	$R_{t,m}$	10 m Ω	$C_{t,m}$	2500 F
Battery Pack (4S2P)											
a_0	11.899	a_1	29.020	a_2	-129.510	a_3	299.090	a_4	-366.81	a_5	231.77
a_6	-59.23	b_0	0.526	b_1	-4.720	b_2	28.510	b_3	-83.270	b_4	125.620
b_5	-94.100	b_6	27.670	$R_{t,s}$	40 m Ω	$C_{t,s}$	400 F	$R_{t,m}$	8 m Ω	$C_{t,m}$	3000 F
UC Pack (8S1P)											
C_u	(2.17 v_u +188.6) F			R_{sc}	10 m Ω	R_{pc}	3 k Ω				
UC Pack (4S2P)											
C_u	(12.39 v_u +591.2) F			R_{sc}	8 m Ω	R_{pc}	2 k Ω				
DC-DC Converter											
R_{mos}	5 m Ω	L	200 μ H	R_L	100 m Ω	V_F	0.26 V	f_s	100 kHz	C_{out}	2000 μ F
Q_{mos}	26 nC	R_{out}	50 m Ω	R_{F1}	20 m Ω	R_{sw}	100 m Ω	R_{D1}	12 m Ω		
Sampling resistor											
R_{s1}	10 m Ω	R_{s2}	100 m Ω	R_{s3}	10 m Ω						

on-board resistor R_{out} , as shown in Fig. 5b. R_{F1} and R_{SW} are the resistances of the fuse and manual power on/off switch on the DC-DC converter board, respectively. The resistance values for the above additional components are also listed in Table II. Thus the duty cycle of the DC-DC converter d'_s and the ESR ratio K' for the real experimental HESS should be calculated as

$$d'_s = 1 - \frac{V_{o,b} + \sqrt{V_{o,b}^2 - 4(R_s + R_{s1})I_{l,a}V_{bus}}}{2V_{bus}}, \quad (30)$$

$$K' = \frac{R_s}{(1-d'_s)^2} + \frac{R_L + d'_s R_{mos} + R_{s1} + R_{F1}}{(1-d'_s)^2} + \frac{R_{sc}}{R_{sc}} + \frac{R_{D1} + R_{out} + R_{sw} + R_{s2}}{R_{sc}}, \quad (31)$$

and C_d^* can be obtained using (21) by replacing K with K' .

B. Pulsed current load

An ideal pulsed current load is first used, in which $I_{l,max}=2.5$ A, $I_{l,min}=0$ A, $T=10$ s, and $D=0.4$. The initial voltages of the battery and UC packs are 7.64 V and 14.80 V, respectively. From (21),(30)-(31), K' is 128 and C_d^* is 0.008. The optimal C_d^* after dropping the assumption of the constant DC-DC duty cycle is obtained by using MATLAB function `fminunc`. It is interesting to find that the optimal C_d^* is also 0.008. This result indicates that the approximation under the assumption of the constant duty cycle is reasonable for the current experimental setup. Figs. 7 and 8 show the simulation and experiment results under a zero C_d , by which the battery pack only provides the average load current through the DC-DC converter, and the UC pack supplies the entire dynamic load current. The simulation well represents the dynamics of the real experimental system. Besides, the duty cycle of the DC-DC converter and the DC bus voltage (i.e., the UC pack

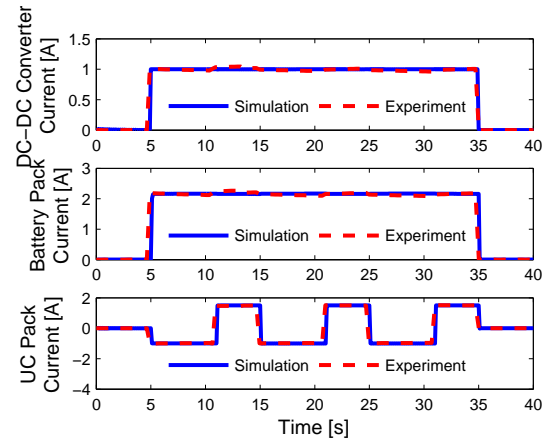


Fig. 7. The currents of the battery pack, the DC-DC Converter, and the UC pack under the pulsed current load and a zero C_d .

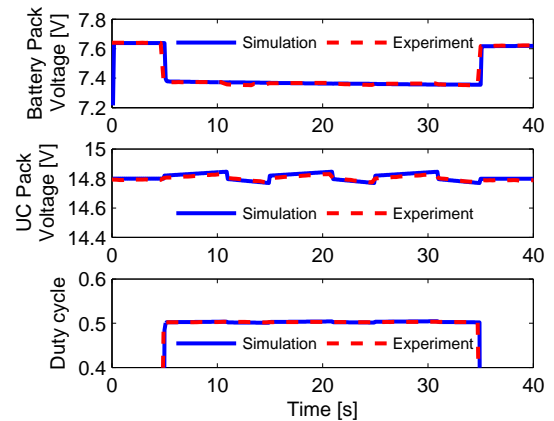


Fig. 8. The voltages of battery and UC packs, and the duty cycle of DC-DC converter under the pulsed current load and a zero C_d .

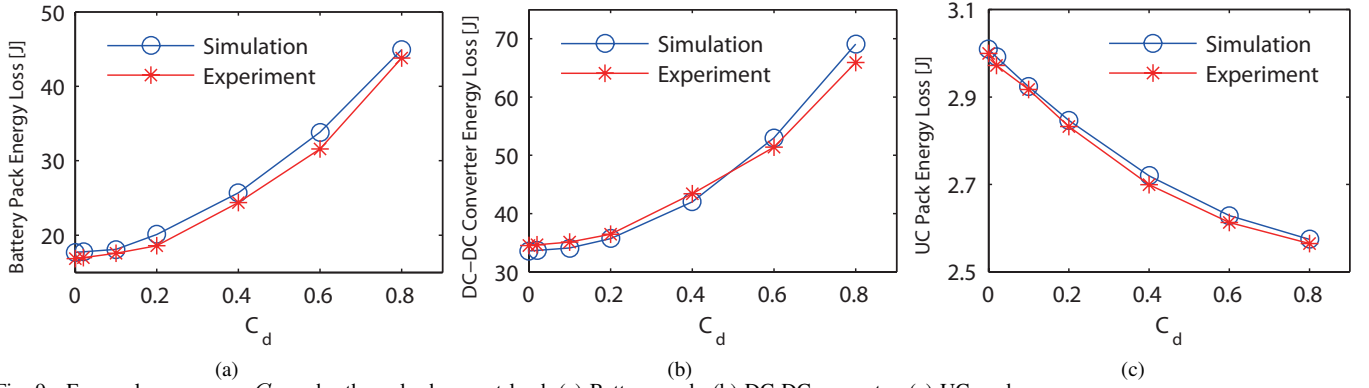


Fig. 9. Energy losses versus C_d under the pulsed current load. (a) Battery pack. (b) DC-DC converter. (c) UC pack.

voltage) are almost constant. This observation is in accordance with the assumptions in section III-A.

Fig. 9 shows the energy losses with a varying C_d from 0 to 0.8. The figure shows that more dynamic current from the battery pack through the DC-DC converter (i.e., an increasing C_d), more energy losses in the two components. On the contrary, the energy loss in the UC pack decreases with an increasing C_d . Since the energy loss in the UC pack is quite small compared to the energy losses in the battery pack and the DC-DC converter, the optimal C_d^* is a small but non-zero number. The relationship between the overall energy loss and C_d is plotted in Fig. 10. Due to the unavoidable sampling noise, the overall system energy loss with small C_d 's between 0 and 0.02 is numerically calculated, as shown in the enlarged subfigure. The optimal C_d^* is about 0.008 that well matches its calculated value. In Fig. 10 the difference between the simulation and experimental results becomes larger with a bigger C_d such as 0.8. A big C_d requires the battery pack to provide the most of dynamic load current, i.e., a large and fast-changing current. Thus in practice it is difficult for the real DC-DC converter to exactly follow the reference current command. This control error mainly contributes to the enlarged difference under big C_d 's. For example, in Fig. 9(b) the difference of the energy loss in DC-DC converter is 3.1 J when C_d is 0.8. Meanwhile, the difference in the overall energy loss is 4.2 J under $C_d=0.8$.

As mentioned in the introduction section, the methodology developed in this paper is a general one, which can be extended to analyze other battery-UC HESS topologies. For reference purposes, the energy loss of an alternative topology, a capacitor semi-active HESS, is discussed here. In this HESS, the battery pack (4S2P) is directly connected to the load and the DC-DC converter is placed between the UC pack (4S2P) and the load. Their parameters are also listed in Table II. The initial voltages of the battery and UC packs are now 14.80 V and 7.64 V, respectively. The calculation of the optimal current distribution coefficient $C_d^{*''}$ is modified accordingly for the

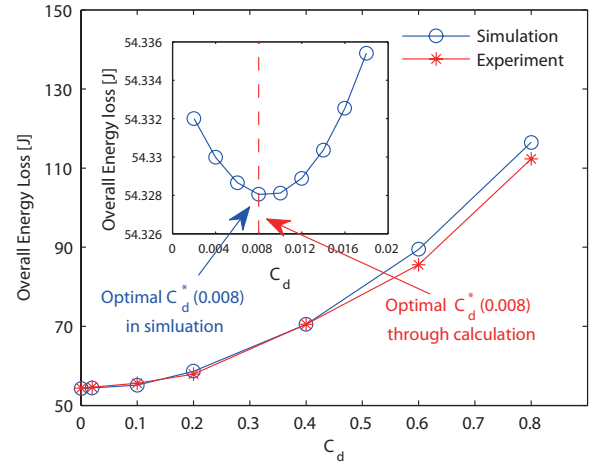


Fig. 10. Overall energy loss of battery semi-active HESS versus C_d under the pulsed current load.

capacitor semi-active HESS, as shown in following equations:

$$R_b^{*''} = R_s'', \quad R_u^{*''} = \frac{R_{sc}''}{(1 - d_s'')^2},$$

$$R_d^{*''} = \frac{R_L + R_{mos} + R_{s1} + R_{F1}}{(1 - d_s'')^2} + R_{out} + R_{sw} + R_{s2},$$

$$d_s'' = 1 - \frac{V_{o,u}''}{V_{o,b}'' - I_{l,a} R_s''}, \quad K'' = \frac{R_b^{*''}}{R_d^{*''} + R_u^{*''}}, \quad (32)$$

$$C_d^{*''} = \frac{1}{1 + K''}. \quad (33)$$

Here the term of V_F/i_d is eliminated in calculating the DC-DC converter's ESR [refer to (11)]. It is because in the capacitor semi-active topology a bi-directional buck-boost DC-DC converter is needed to charge and discharge the UC pack [7]. Thus the diode in the previous boost DC-DC converter is substituted by a MOSFET. As shown in Fig. 11, the calculated and simulated $C_d^{*''}$'s are both 0.752, and their existence can be clearly observed in the two curves. The difference between the simulation and experimental results becomes large with a small C_d such as zero, under which the UC pack is required to provide large and fast-changing current. Again for the real DC-DC converter (connected with the UC pack here) it is difficult to exactly follow its reference current command. Besides, the

optimal C_d^{**} after dropping the assumption of a constant DC-DC duty cycle is searched again using MATLAB function `fminunc`. It is interesting to find that C_d^{**} is still 0.752. The above results for the alternative capacitor semi-active topology well illustrate the generality of the proposed methodology.

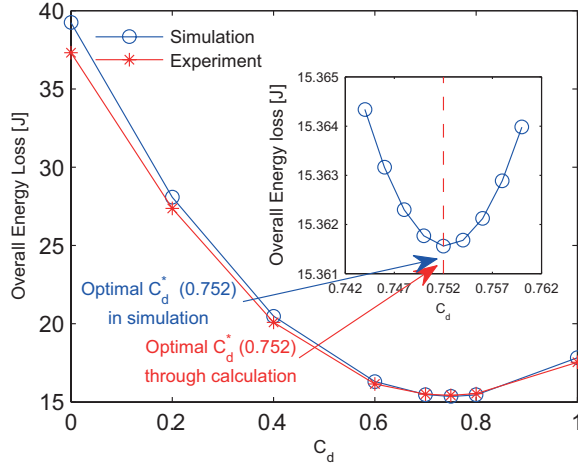


Fig. 11. Overall energy loss of capacitor semi-active HESS versus C_d under the pulsed current load.

C. Sensitivity Analysis

As shown in (16)-(18), the overall energy loss E_{loss} of the example battery semi-active HESS relates to the characteristics of the battery and UC packs. Fig. 12 shows the partial derivatives of (16) with respect to internal resistances and OCVs of the battery and UC packs (R_s , R_{sc} , $V_{o,b}$, and $V_{o,u}$), respectively, when C_d varies from 0 to 1. It can be seen that the internal resistance of the battery pack R_s is the key factor to affect the overall energy loss of the HESS. With a larger C_d the influence of R_s becomes more dominant. This is because more dynamic load current needs to be provided by the battery pack and usually R_s is much larger than R_{sc} . At the same time, the influence of R_{sc} diminishes with an increasing C_d . The two OCVs, $V_{o,b}$ and $V_{o,u}$, affect the battery current through changing the duty cycle of the DC-DC converter. The partial derivative with respect to $V_{o,b}$ is negative because a higher $V_{o,b}$ leads to a smaller battery current at certain power and thus less energy loss from the battery pack; while the positive partial derivative with respect to $V_{o,u}$ can be similarly explained.

D. Influence of sizing

In order to facilitate the theoretical discussion, the size of the UC pack in the current experimental setup is large enough to maintain a nearly constant DC bus voltage. However, in real applications there are physical constraints such as on weight and space. With a small-sized UC pack, the DC bus voltage cannot be assumed to be constant any longer [19]. Fig. 13 shows the magnitude of DC bus voltage variation and the overall energy loss of the HESS versus the capacitance of the UC pack under the optimal C_d^* s in the simulation. Here the internal resistance R_{sc} and leak-current resistance R_{pc} of the UC pack is assumed to be inversely proportional to its

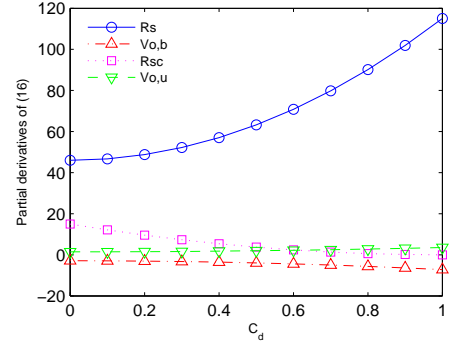


Fig. 12. The partial derivatives of the overall energy loss with respect to R_s , R_{sc} , $V_{o,b}$, and $V_{o,u}$.

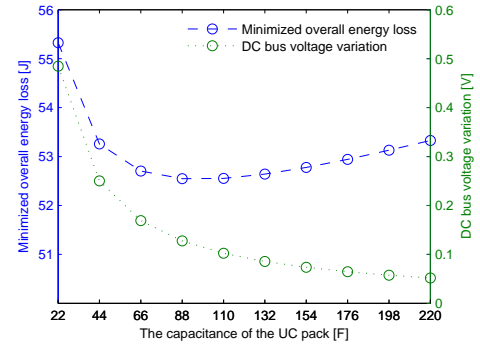


Fig. 13. The magnitude of DC bus voltage variation and the overall energy loss of the battery semi-active HESS versus the capacitance of the UC pack under the optimal C_d^* s.

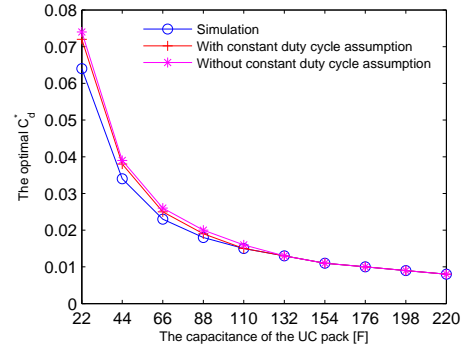


Fig. 14. The comparison of the optimal C_d^* s through calculation and simulation.

specific capacitance [see Table II]. In the figure, the overall energy loss is minimized when the capacitance of the UC pack is 88 F. This is because for a smaller-sized UC pack the loss caused by R_{sc} increases due to a bigger R_{sc} ; while for the loss from R_{pc} the tendency is opposite. On the other hand, the magnitude of the DC bus voltage variation keeps increasing with a smaller UC pack. In a specific application the sizing of the UC pack should be determined based on the performance and design requirements of the target HESS.

Fig. 14 compares the accurate optimal C_d^* s through the simulation and C_d^* s calculated without/with dropping the assumption of a constant duty cycle of the DC-DC converter.

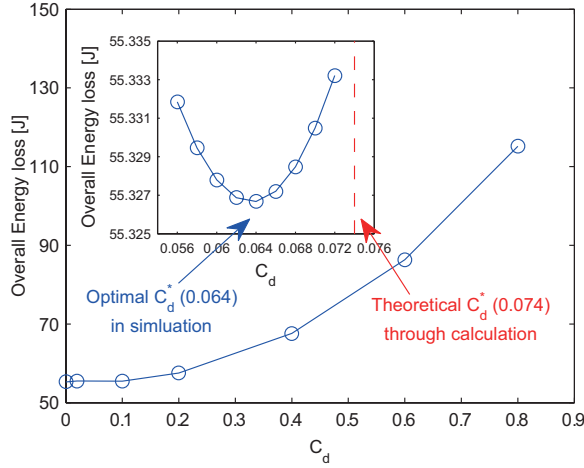


Fig. 15. Overall energy loss versus C_d using a small-sized UC pack in simulation.

The error between the accurate C_d^* and the two calculated C_d^* 's becomes obvious when the capacitance of the UC pack is below 110 F. This is mainly because the variation of the DC bus voltage is too large to assume a constant DC bus voltage; while the calculated C_d^* 's still well predict the trend in the variation of the actual C_d^* . It should be noted that the two calculated C_d^* 's are very close. In the battery-UC HESSs, usually the internal resistance of the battery pack is much larger than that of the UC pack. Thus the C_d^* 's are always small numbers. This leads to a small variation of the battery current around the average current, and limited variation range of the duty cycle of the DC-DC converter.

Fig. 15 shows the simulated overall energy loss of the HESS when the capacitance of the UC pack is 22 F (i.e., 1/10 of that of the original UC pack) under the pulsed current load. The relationship between the overall energy loss and C_d is still close to a quadratic function. The optimal C_d^* is derived as 0.072 using (21), (30)-(31). Based on (9), the UC pack is first charged and then discharged to its initial voltage, 14.80 V here, under the pulsed current load. However, with the limited capacity of the UC pack, the average DC bus voltage (i.e., the UC pack voltage) is higher than the previously assumed 14.80 V. Based on (30) and (31), the actual average duty cycle of the DC-DC converter d_s^* and the resistance ratio K' become larger than their calculated values. And they vary with different C_d . Thus, for the small-sized UC pack, its optimal C_d^* (=0.064) in simulation is smaller than the calculated value, 0.072.

E. Influence of large $R_{t,s}$ and $R_{t,m}$

It should be noted that for some lithium-ion batteries their $R_{t,s}$ and $R_{t,m}$ may be relatively large under certain conditions. For example, the experimental results in [31] show that $R_{t,s}$ and $R_{t,m}$ of a lithium-iron-phosphate battery at -20°C are 100 and 20 times as large as those at 20°C , respectively; while $C_{t,s}$ and $C_{t,m}$ at -20°C become one-fourth of those at 20°C . Numerical simulation is carried out to search the optimal C_d^* in which the values of $R_{t,s}$, $R_{t,m}$, $C_{t,s}$, and $C_{t,m}$ are multiplied by 100, 20, $\frac{1}{4}$, and $\frac{1}{4}$, respectively. The result shows that the optimal C_d^* is 0.006, a value smaller than its

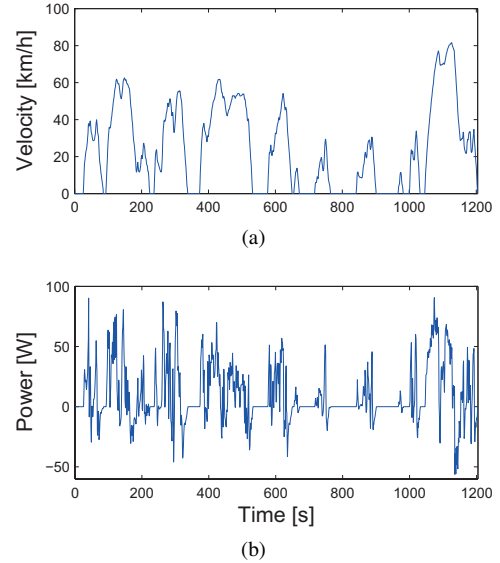


Fig. 16. Velocity and downsized power profiles of the JC08 driving cycle. (a) Velocity. (b) Power.

calculated one, 0.008 [refer to (21)]. This is because the energy losses caused by $R_{t,s}$ and $R_{t,m}$ are more obvious and thus the actual R_b^* becomes larger (i.e., an increased $P_{loss,b}$) [refer to (12)]. Meanwhile, the calculated optimal C_d^* still gives a good prediction.

F. Realistic test cycle

Here instead of the ideal pulsed current load, a more realistic testy cycle, the Japanese JC08 cycle, is applied. The velocity profile of the JC08 cycle is shown in Fig. 16(a) that was designed to represent a congested city driving [32], [33]. Its corresponding power profile is then scaled down to match the power capability of the current experimental battery semi-active HESS [see Fig. 16(b)]. Figs. 17 and 18 show the simulation and experimental results (currents and voltages) under a zero C_d . It can be seen that the dynamic models well represent the dynamics of the real experimental HESS under the realistic JC08 cycle. Since the UC pack is only a temporary energy source, after one entire cycle the voltage of the UC pack (i.e. its stored energy) should be the same as its initial voltage; if not, the UC pack will be charged until its voltage reaches the initial voltage. In real experiments there are unavoidable measurement and control errors. And the duration of the JC08 cycle is relatively long, 1204 seconds. The accumulated errors cause different stopping times for the current/voltage responses in simulation and experiment.

As shown in Fig. 19, a similar relationship exists between the overall energy loss and C_d . The theoretical optimal C_d^* now from (21),(30)-(31) is 0.008, which is again validated by the simulation results, as shown in the enlarged subfigure. When C_d is large, the difference between the simulation and experiment results becomes obvious. It is because for a large C_d such as 0.6 battery pack is required to provide the most of the dynamic load current, i.e., a large fast-changing current [refer to (7)]. Thus again it is difficult for the real DC-DC converter to exactly follow the reference current command.

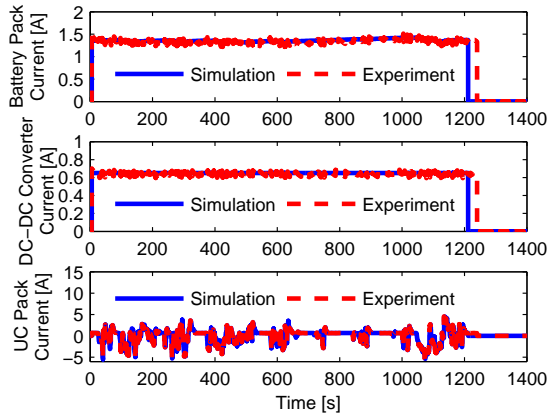


Fig. 17. The currents of the battery pack, the DC-DC converter, and UC pack under a zero C_d and the JC08 test cycle.

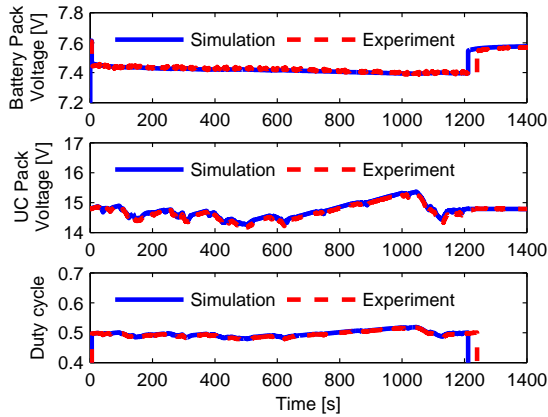


Fig. 18. The voltages of the battery and UC packs, and the duty cycle of the DC-DC converter under a zero C_d and the JC08 test cycle.

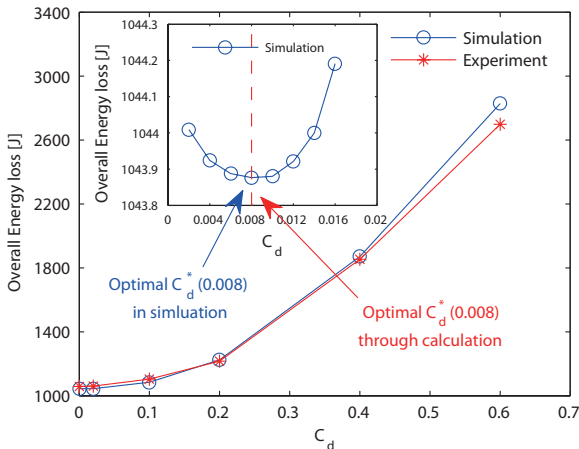


Fig. 19. Overall energy loss versus C_d under the JC08 test cycle.

This control error mainly contributes to the enlarged difference between the two results. Besides, under the realistic JC08 test cycle, the variation of the DC-DC converter's duty cycle is relatively large. This variation causes the deviation from the ideal quadratic relationship between the overall energy loss of the HESS and C_d [refer to (16)]. Finally, as discussed in section III-C, for a general profile such as the JC08 cycle it is difficult to analytically solve the optimal C_d^* after dropping the assumption of a constant duty cycle of the DC-DC converter. Meanwhile, the more general solution of C_d^* using (29) provides a hint of developing a new real time optimal control method for the HESS.

V. CONCLUSION

In this paper, the energy loss of an example battery semi-active HESS is analyzed based on the ESRs and a pulsed current load profile. It is theoretically proved that the optimal current distribution is solely determined by the ESR ratio of the battery pack and the DC-DC converter to the UC pack. Due to the large difference in the internal resistances, for the battery semi-active HESS a quasi-optimal current distribution can be simply letting the battery pack provide the average load current, and thus the UC pack supplies the entire dynamic load current. This fundamental result clearly explains that besides the well-known purpose of battery protection, in order to minimize the energy loss, the UC pack is also required to provide most of the dynamic load current. Both the simulation and experimental results well match the calculated results. This consistency in turn verifies the correctness of the theoretical discussion and the accuracy of the ESR models. Additional simulation results using a small-sized UC pack show that the overall energy loss is still close to a quadratic function of the current distribution coefficient C_d , but the optimal C_d^* is different from its theoretical value. An alternative HESS topology (such as the capacitor semi-active HESS) and a more realistic test cycle may also influence the relationship between the overall energy loss and C_d . Meanwhile, the calculated and simulated optimal C_d^* 's still match with each other well. This good matching indicates that the methodology developed in this paper can provide a general and important guideline for discussing optimized design and control of real battery-UC HESSs. The future work may include extending the methodology to analyze other battery-ultracapacitor HESSs and developing a realtime control strategy based on the results in this paper.

REFERENCES

- [1] A. Khaligh and Z. Li, "Battery, ultracapacitor, fuel cell, and hybrid energy storage systems for electric, hybrid electric, fuel cell, and plug-in hybrid electric vehicles: State of the art," *IEEE Trans. Veh. Technol.*, vol. 59, pp. 2806–2814, Jul. 2010.
- [2] J. Cao and A. Emadi, "A new battery/ultracapacitor hybrid energy storage system for electric, hybrid, and plug-in hybrid electric vehicles," *IEEE Trans. Power Electron.*, vol. 27, pp. 122–132, Jan. 2012.
- [3] P. Sharma and T. Bhatti, "A review on electrochemical double-layer capacitors," *Energy Convers. Manage.*, vol. 51, no. 12, pp. 2901–2912, 2010.
- [4] R. Kötz and M. Carlen, "Principles and applications of electrochemical capacitors," *Electrochim. Acta*, vol. 45, no. 15, pp. 2483–2498, 2000.

- [5] A. Burke and M. Miller, "The power capability of ultracapacitors and lithium batteries for electric and hybrid vehicle applications," *J. Power Sources*, vol. 196, no. 1, pp. 514–522, 2011.
- [6] A. Burke, "Ultracapacitors: why, how, and where is the technology," *J. Power Sources*, vol. 91, no. 1, pp. 37–50, 2000.
- [7] A. Kuperman and I. Aharon, "Battery-ultracapacitor hybrids for pulsed current loads: A review," *Renew Sust. Energy Rev.*, vol. 15, pp. 981–992, Feb. 2011.
- [8] A. W. Stienecker, T. Stuart, and C. Ashtiani, "An ultracapacitor circuit for reducing sulfation in lead acid batteries for mild hybrid electric vehicles," *J. Power Sources*, vol. 156, no. 2, pp. 755–762, 2006.
- [9] D. Cericola, P. Ruch, R. Kötzt, P. Novák, and A. Wokaun, "Simulation of a supercapacitor/li-ion battery hybrid for pulsed applications," *J. Power Sources*, vol. 195, no. 9, pp. 2731–2736, 2010.
- [10] M. Ortúzar, J. Moreno, and J. Dixon, "Ultracapacitor-based auxiliary energy system for an electric vehicle: Implementation and evaluation," *IEEE Trans. Ind. Electron.*, vol. 54, no. 4, pp. 2147–2156, 2007.
- [11] O. C. Onar and A. Khaligh, "A novel integrated magnetic structure based dc/dc converter for hybrid battery/ultracapacitor energy storage systems," *IEEE Trans. Smart Grid*, vol. 3, no. 1, pp. 296–307, 2012.
- [12] J. Moreno, M. E. Ortúzar, and J. W. Dixon, "Energy-management system for a hybrid electric vehicle, using ultracapacitors and neural networks," *IEEE Trans. Ind. Electron.*, vol. 53, pp. 614–623, Apr. 2006.
- [13] X. Zhang, C. C. Mi, A. Masrur, and D. Daniszewski, "Wavelet-transform-based power management of hybrid vehicles with multiple on-board energy sources including fuel cell, battery and ultracapacitor," *J. Power Sources*, vol. 185, no. 2, pp. 1533–1543, 2008.
- [14] O. Erdinc, B. Vural, and M. Uzunoglu, "A wavelet-fuzzy logic based energy management strategy for a fuel cell/battery/ultra-capacitor hybrid vehicular power system," *J. Power sources*, vol. 194, pp. 369–380, Oct. 2009.
- [15] M. Zandi, A. Payman, J.-P. Martin, S. Pierfederici, B. Davat, and F. Meibody-Tabar, "Energy management of a fuel cell/supercapacitor/battery power source for electric vehicular applications," *IEEE Trans. Veh. Technol.*, vol. 60, pp. 433–443, Feb. 2011.
- [16] D. Rotenberg, A. Vahidi, and I. Kolmanovsky, "Ultracapacitor assisted powertrains: Modeling, control, sizing, and the impact on fuel economy," *IEEE Trans. Control Syst. Technol.*, vol. 19, pp. 576–589, May 2011.
- [17] O. Laldin, M. Moshirvaziri, and O. Trescases, "Predictive algorithm for optimizing power flow in hybrid ultracapacitor/battery storage systems for light electric vehicles," *IEEE Trans. Power Electron.*, vol. 28, pp. 3882–3895, Aug. 2013.
- [18] M.-E. Choi, S.-W. Kim, and S.-W. Seo, "Energy management optimization in a battery/supercapacitor hybrid energy storage system," *IEEE Trans. Smart Grid*, vol. 3, pp. 463–472, Mar. 2012.
- [19] A. Kuperman, I. Aharon, S. Malki, and A. Kara, "Design of a semi-active battery-ultracapacitor hybrid energy source," *IEEE Trans. Power Electron.*, vol. 28, pp. 806–815, Feb. 2013.
- [20] S. Lu, K. A. Corzine, and M. Ferdowsi, "A unique ultracapacitor direct integration scheme in multilevel motor drives for large vehicle propulsion," *IEEE Trans. Veh. Technol.*, vol. 56, no. 4, pp. 1506–1515, Jul. 2007.
- [21] M. Chen and G. A. Rincon-Mora, "Accurate electrical battery model capable of predicting runtime and IV performance," *IEEE Trans. Energy Convers.*, vol. 21, no. 2, pp. 504–511, Jun. 2006.
- [22] R. C. Kroeze and P. T. Krein, "Electrical battery model for use in dynamic electric vehicle simulations," in *Proc. IEEE Power Electronics Specialists (PESC'2008)*, Rhodes, Greece, Jun. 2008, pp. 1336–1342.
- [23] W. Waag, S. Käbitz, and D. U. Sauer, "Experimental investigation of the lithium-ion battery impedance characteristic at various conditions and aging states and its influence on the application," *Applied Energy*, vol. 102, pp. 885–897, 2013.
- [24] M. Mellincovsky, A. Kuperman, C. Lerman, S. Gadelovits, I. Aharon, N. Reichbach, G. Geula, and R. Nakash, "Performance and limitations of a constant power-fed supercapacitor," *IEEE Trans. Energy Convers.*, vol. 29, no. 2, pp. 445–452, Jun. 2014.
- [25] M. S. Chan, K. Chau, and C. Chan, "Effective charging method for ultracapacitors," *Journal of Asian Electric Vehicles*, vol. 3, pp. 771–776, Dec. 2005.
- [26] Y. Choi, N. Chang, and T. Kim, "DC-DC converter-aware power management for low-power embedded systems," *IEEE Trans. Comput.-Aid. Des.*, vol. 26, pp. 1367–1381, Aug. 2007.
- [27] T. Eichhorn, "Boost converter efficiency through accurate calculations," *Power Electron.*, vol. 34, pp. 30–35, Sep. 2008.
- [28] A. Kuperman, I. Aharon, A. Kara, and S. Malki, "A frequency domain approach to analyzing passive battery-ultracapacitor hybrids supplying

periodic pulsed current loads," *Energy Convers. Manag.*, vol. 52, no. 12, pp. 3433–3438, 2011.

- [29] S. Abu-Sharkh and D. Doerffel, "Rapid test and non-linear model characterisation of solid-state lithium-ion batteries," *J. Power Sources*, vol. 130, pp. 266–274, May 2004.
- [30] W. Lajnef, J.-M. Vinassa, O. Briat, S. Azzopardi, and E. Woïrgard, "Characterization methods and modelling of ultracapacitors for use as peak power sources," *J. Power Sources*, vol. 168, pp. 553–560, Jun. 2007.
- [31] L. Liao, P. Zuo, Y. Ma, X. Chen, Y. An, Y. Gao, and G. Yin, "Effects of temperature on charge/discharge behaviors of LiFePO₄ cathode for li-ion batteries," *Electrochim. Acta*, vol. 60, pp. 269–273, 2012.
- [32] K. Kiyota, H. Sugimoto, and A. Chiba, "Comparison of energy consumption of SRM and IPMSM in automotive driving schedules," in *Proc. IEEE Energy Conversion Congress and Exposition (ECCE'12)*, Raleigh, NC, USA, Sep. 2012, pp. 853–860.
- [33] S. Chopra and P. Bauer, "Driving range extension of EV with on-road contactless power transfer-a case study," *IEEE Trans. Ind. Electron.*, vol. 60, no. 1, pp. 329–338, 2013.



Chen Zhao (S'14) received the B.S. degree from East China University of Science and Technology, Shanghai, China, in 2011. He is currently working toward Ph.D. degree in electrical and computer engineering, University of Michigan-Shanghai Jiao Tong University Joint Institute, Shanghai Jiao Tong University, Shanghai, China.

His research interests include testing, modeling, and control of hybrid energy systems.



He Yin (S'13) received the B.S. degree in the electrical and computer engineering from University of Michigan-Shanghai Jiao Tong University Joint Institute, Shanghai Jiao Tong University, Shanghai, China in 2012. He is currently working toward Ph.D. degree at the same institute.

His research interests include optimization and control of alternative energy systems such as energy storage systems using ultracapacitors and wireless power transfer systems.



Zhongping Yang (M'07) received his B. Eng. degree from Tokyo University of Mercantile Marine, Tokyo, Japan, in 1997, and the M.S. and Ph.D. degrees both in the electrical engineering from University of Tokyo, Tokyo, Japan, in 1999 and 2002, respectively.

He is currently a professor at the School of Electrical Engineering, Beijing Jiaotong University, Beijing, China. His research interests include high-speed rail system, traction and regenerative braking technologies, and wireless power transfer for light rail vehicles. Dr. Yang won the 10th "Zhan Tianyou" Youth Award of Railway Science and Technology due to his contribution to China's high-speed railway technology in 2010 and the Award of Excellent Popular Science and Technology Books in China in 2011.



Chengbin Ma (M'05) received the B.S.E.E. (Hons.) degree from East China University of Science and Technology, Shanghai, China, in 1997, and the M.S. and Ph.D. degrees both in the electrical engineering from University of Tokyo, Tokyo, Japan, in 2001 and 2004, respectively.

He is currently an assistant professor of electrical and computer engineering with the University of Michigan-Shanghai Jiao Tong University Joint Institute, Shanghai Jiao Tong University, Shanghai, China. He is also with a joint faculty appointment in School of Mechanical Engineering, Shanghai Jiao Tong University. Between 2006 and 2008, he held a post-doctoral position with the Department of Mechanical and Aeronautical Engineering, University of California Davis, California, USA. From 2004 to 2006, he was a R&D researcher with Servo Laboratory, Fanuc Limited, Yamanashi, Japan. His research interests include networked hybrid energy systems, wireless power transfer, and mechatronic control.